

Aided Inertial Navigation: Unified Feature Representations and Observability Analysis

Yulin Yang and Guoquan Huang

Abstract—Extending our recent work [1] that focuses on the observability analysis of aided inertial navigation systems (INS) using *homogeneous* geometric features including points, lines and planes, in this paper, we complete the analysis for the general aided INS using different *combinations* of geometric features (i.e., points, lines and planes). We analytically show that the linearized aided INS with different feature combinations generally possesses the same observability properties as those with same features, i.e., 4 unobservable directions, corresponding to the global yaw rotation and the global position of the sensor platform. During the analysis, we particularly propose a novel minimal representation of line features, i.e., the “closest point” parameterization, which uses a 4D Euclidean vector to describe a line and is proved to preserve the same observability properties. Based on that, for the first time, we provide two sets of *unified* representations for points, lines and planes, i.e., the quaternion form and the closest point (CP) form, and perform extensive observability analysis with analytically-computed Jacobians for these unified parameterizations. We validate the proposed CP representations and observability analysis with Monte-Carlo simulations, in which EKF-based vision-aided INS (VINS) with combinations of geometrical features in CP form are developed and compared.

I. INTRODUCTION AND RELATED WORK

Inertial navigation systems (INS) have become ubiquitous and found their ways in many application domains from augmented reality to autonomous navigation. However, low-cost inertial measurement units (IMUs) suffer from non-negligible measurement noises and time-varying biases. Pose estimation solely based on IMU measurements (angular velocity and linear acceleration) will result in large errors in a short period of time. For this reason, great efforts have been devoted to INS aided with additional sensors such as camera [2] and sonar [3], in order to achieve higher localization accuracy.

As low-cost and light-weight optical cameras are one of the ideal aiding sources for INS, many different state estimation algorithms for vision-aided INS (VINS) have been developed (e.g., [4]–[10] and references therein). Among them, extended Kalman filter (EKF)-based methods are among the most popular algorithms, such as multi-state constrained Kalman filter (MSCKF) [2], observability constrained (OC)-EKF [4], [11], right invariant error (RI)-EKF [12].

System observability plays important roles for state estimation [13]. First of all, understanding a system observability

provides a deep insight about the system’s geometrical properties [4], [14], [15] and determines the minimal measurement modalities or state parameters needed to initialize an estimator. Secondly, it can be used to identify degenerate motions [1], [16] that cause additional unobservable directions and should be avoided or alerted in real-world applications. Thirdly, the observability-based methodologies used in OC-EKF [11] and OC-VINS [4] that enforce the correct observability properties, can be adopted to improve estimation consistency. Last but not least important, analytical measurement Jacobians for aided INS estimators, can be verified through the observability analysis process.

For these reasons, in the past decade, significant research efforts have been devoted on the observability analysis for INS. Among them, Martinelli [17] has proved that biases, velocity, and roll and pitch angles in VINS are observable, while Hesch et al. [4] and Kottas et al. [18] have analytically derived the observability matrix for linearized VINS and shown that there are 4 unobservable directions for VINS with point features. However, the vast majority of VINS estimators and their related observability analysis have focused *only* on point features, albeit using line [19]–[23] and plane [24]–[27] features has recently been reviving. Different parameterizations of line features in VINS have been considered. A unit quaternion with a distance scalar to represent line features was used in VINS [20] where observability analysis for linearized VINS with lines was also performed. Plücker representation with orthonormal error states for lines [28] were adopted in point and line based VINS [21], [22]. Two ending points of line segment to represent line features were used in recent point/line-based MSCKF [23]. On the other hand, plane features were also exploited in recent SLAM and VINS systems. For example, the VINS observability with point features and plane features with known orientation was studied in [25], and the 2D LiDAR aided INS (L-INS) was also developed by estimating the perpendicular structural planes within structured buildings [24]. The dense planar visual-inertial SLAM system has recently been developed [26] which incorporates plane features extracted from dense point clouds and represented in quaternion form as in [29]. In contrast, in our prior work [30], we have introduced the closest point (CP) representation of planes for aided INS, which was successfully employed in our recent 3D LiDAR-inertial plane SLAM system [27].

One particular challenge when incorporating different geometrical features into state estimation is to find appropriate representations, especially for their error states. As seen

This work was partially supported by the University of Delaware (UD) College of Engineering, the NSF (IIS-1566129), the DTRA (HDTRA1-16-1-0039), and Google.

The authors are with the Department of Mechanical Engineering, University of Delaware, Newark, DE 19716, USA. Email: {yuyang, ghuang}@udel.edu

from the above discussion, while different parameterizations for point, line and planes have been used, there is still a lack of an unified representation for all these geometrical features, which is of particular interest when using all different features in a single estimator. To this end, Nardi et al. [31] have tried to find a unified representation for different geometrical primitives with a uniform data structure and the operation between different geometrical features can be decided by a multiplication table. However, it is not clear how to incorporate measurement uncertainty into this representation, which is necessary for state estimation.

In this paper, to bridge this gap, by fully understanding the most commonly used parameterizations for different geometrical features, we propose two sets of *unified* representations for point, line and plane: (i) the unit quaternion based parameterization, and (ii) the closest point based parameterization. Note that each unified representation has a minimal feature error state and the related measurement uncertainties can be easily incorporated into an INS estimator. Moreover, based on our recent work [1] where we performed the observability analysis for linearized aided INS with homogeneous point, line and plane features separately, we analyze the observability for linearized aided INS with *combinations* of point, line and plane features all in our proposed CP form and examine their corresponding unobservable subspace. Specifically, the main contributions of this paper include:

- We introduce two sets of unified representations of both quaternion and CP forms for points, lines and planes. In particular, the CP form of lines is proposed for the first time, which is a minimal parameterization with a 4D Euclidean vector to represent a line and its error state.
- We perform complete observability analysis for aided INS with points, lines and planes in quaternion (or CP) form and show that the aided INS has the same unobservable properties given the analytically computed measurement Jacobians with the proposed unified parameterization. We also prove that aided INS with combination of all the geometrical features in CP form generally has the same 4 unobservable directions.
- We conduct extensive Monte-Carlo simulations to validate the proposed CP representation and observability analysis for the aided INS with combinations of geometrical features.

II. AIDED INERTIAL NAVIGATION SYSTEM

In this section, we briefly describe the system and measurement models for the aided INS with different geometrical features. The state vector of the aided INS contains the current IMU state \mathbf{x}_I and the feature state ${}^G\mathbf{x}_{\text{feat}}$:

$$\mathbf{x} = \begin{bmatrix} \mathbf{x}_I^T & {}^G\mathbf{x}_{\text{feat}}^T \end{bmatrix}^T = \begin{bmatrix} {}^I\bar{q}^T & \mathbf{b}_g^T & {}^G\mathbf{v}_I^T & \mathbf{b}_a^T & {}^G\mathbf{p}_I^T & {}^G\mathbf{x}_{\text{feat}}^T \end{bmatrix}^T \quad (1)$$

where ${}^I\bar{q}$ is a unit quaternion represents the rotation between the current IMU frame $\{I\}$ and the global frame $\{G\}$, and ${}^I_G\mathbf{R}(\bar{q})$ is the corresponding rotation matrix. \mathbf{b}_g and \mathbf{b}_a represent the gyroscope and accelerometer biases, respectively, while ${}^G\mathbf{v}_I$ and ${}^G\mathbf{p}_I$ denote the current IMU velocity and

position in the global frame. ${}^G\mathbf{x}_{\text{feat}}$ generically denotes the features of different geometric types such as points, lines and planes. For simplicity, the aiding exteroceptive sensor frame is assumed to coincide with the IMU frame in this paper.

A. System Kinematic Model

The motion model of the system can be described as [32]:

$$\begin{aligned} {}^I_G\dot{\bar{q}}(t) &= \frac{1}{2}\Omega\left({}^I\omega(t)\right){}^I_G\bar{q}(t), \quad {}^G\dot{\mathbf{p}}_I(t) = {}^G\mathbf{v}_I(t), \quad {}^G\dot{\mathbf{v}}_I(t) = {}^G\mathbf{a}(t) \\ \dot{\mathbf{b}}_g(t) &= \mathbf{n}_{wg}(t), \quad \dot{\mathbf{b}}_a(t) = \mathbf{n}_{wa}(t), \quad {}^G\dot{\mathbf{x}}_{\text{feat}}(t) = \mathbf{0}_{m \times 1} \end{aligned} \quad (2)$$

where ω and \mathbf{a} are the angular velocity and linear acceleration, respectively. \mathbf{n}_{wg} and \mathbf{n}_{wa} are the zero-mean Gaussian noises driving the IMU gyroscope and accelerometer biases.

m is the dimension of ${}^G\mathbf{x}_{\text{feat}}$, and $\Omega(\omega) \triangleq \begin{bmatrix} -[\omega] & \omega \\ \omega^T & 0 \end{bmatrix}$, with $[\cdot]$ denotes skew symmetric matrix. Hence, the linearized continuous-time error-state equations can be written as:

$$\begin{aligned} \dot{\tilde{\mathbf{x}}}(t) &\simeq \begin{bmatrix} \mathbf{F}_c(t) & \mathbf{0}_{15 \times m} \\ \mathbf{0}_{m \times 15} & \mathbf{0}_m \end{bmatrix} \tilde{\mathbf{x}}(t) + \begin{bmatrix} \mathbf{G}_c(t) \\ \mathbf{0}_{m \times 12} \end{bmatrix} \mathbf{n}(t) \\ &= \mathbf{F}(t)\tilde{\mathbf{x}}(t) + \mathbf{G}(t)\mathbf{n}(t) \end{aligned} \quad (3)$$

where $\tilde{\mathbf{x}} = \mathbf{x} - \hat{\mathbf{x}}$ denotes the errors between the true state \mathbf{x} and its estimate $\hat{\mathbf{x}}$. The error states for quaternion can be described as: $\delta\bar{q} = \bar{q} \otimes \hat{q}^{-1}$ with \otimes represents the quaternion multiplication and $\delta\bar{q} = \begin{bmatrix} \frac{1}{2}\delta\theta^T & 1 \end{bmatrix}^T$. $\mathbf{F}_c(t)$ and $\mathbf{G}_c(t)$ are the continuous-time error-state noise Jacobian matrices, respectively. $\mathbf{n}(t) = \begin{bmatrix} \mathbf{n}_g^T & \mathbf{n}_{wg}^T & \mathbf{n}_a^T & \mathbf{n}_{wa}^T \end{bmatrix}^T$ is modeled as a zero-mean Gaussian process with autocorrelation $\mathbb{E}[\mathbf{n}(t)\mathbf{n}^T(\tau)] = \mathbf{Q}_c\delta(t-\tau)$. Note that $\mathbf{n}_g(t)$ and $\mathbf{n}_a(t)$ are the noise contaminating angular velocity and linear acceleration measurements. The discrete-time state transition matrix $\Phi_{(k+1,k)}$ from time t_k to t_{k+1} can be derived as:

$$\begin{aligned} \Phi_{(k+1,k)} &= \begin{bmatrix} \Phi_I & \mathbf{0}_{15 \times m} \\ \mathbf{0}_{m \times 15} & \Phi_{\text{feat}} \end{bmatrix} \\ &= \begin{bmatrix} \Phi_{I11} & \Phi_{I12} & \mathbf{0}_3 & \mathbf{0}_3 & \mathbf{0}_3 & \mathbf{0}_{3 \times m} \\ \mathbf{0}_3 & \mathbf{I}_3 & \mathbf{0}_3 & \mathbf{0}_3 & \mathbf{0}_3 & \mathbf{0}_{3 \times m} \\ \Phi_{I31} & \Phi_{I32} & \mathbf{I}_3 & \Phi_{I34} & \mathbf{0}_3 & \mathbf{0}_{3 \times m} \\ \mathbf{0}_3 & \mathbf{0}_3 & \mathbf{0}_3 & \mathbf{I}_3 & \mathbf{0}_3 & \mathbf{0}_{3 \times m} \\ \Phi_{I51} & \Phi_{I52} & \Phi_{I53} & \Phi_{I54} & \mathbf{I}_3 & \mathbf{0}_{3 \times m} \\ \mathbf{0}_{m \times 3} & \mathbf{0}_{m \times 3} & \mathbf{0}_{m \times 3} & \mathbf{I}_{m \times 3} & \mathbf{0}_{m \times 3} & \mathbf{I}_m \end{bmatrix} \end{aligned} \quad (4)$$

where Φ_I and Φ_{feat} represents the state transition matrix of the IMU state and the feature state respectively, and the analytical solution can be found in [4].

B. Point Measurements

The point measurements from different sensors in the aided INS can be generically modeled as range and/or bearing measurements [1]:

$$\mathbf{z}_p = \begin{bmatrix} z^{(r)} \\ \mathbf{z}^{(b)} \end{bmatrix} = \begin{bmatrix} \sqrt{{}^I\mathbf{x}_f^T {}^I\mathbf{x}_f + n^{(r)}} \\ \mathbf{h}_b\left({}^I\mathbf{x}_f, \mathbf{n}^{(b)}\right) \end{bmatrix} \simeq \begin{bmatrix} \mathbf{H}_r {}^I\tilde{\mathbf{x}}_f + n^{(r)} \\ \mathbf{H}_b {}^I\tilde{\mathbf{x}}_f + \mathbf{H}_r \mathbf{n}^{(b)} \end{bmatrix} \quad (5)$$

where ${}^I\mathbf{x}_f$ represents a 3D point in IMU frame, \mathbf{H}_r and \mathbf{H}_b are the range and bearing measurement Jacobians with respect to ${}^I\mathbf{x}_f$, \mathbf{H}_n is the noise Jacobian, $n^{(r)}$ and $\mathbf{n}^{(b)}$ are zero-mean Gaussian noises for range and bearing measurements, respectively. To keep presentation concise, we also define $\mathbf{H}_{proj} = \begin{bmatrix} \mathbf{H}_r^\top & \mathbf{H}_b^\top \end{bmatrix}$ (see [1]).

C. Line Measurements

Without loss of generality, we consider the projective line measurements [28], which can be defined as the distance of two ending image points, \mathbf{x}_s and \mathbf{x}_e , to the projected line segment in the image:

$$\mathbf{z}_l = \begin{bmatrix} \frac{\mathbf{x}_s^\top \mathbf{l}}{\sqrt{l_1^2 + l_2^2}} & \frac{\mathbf{x}_e^\top \mathbf{l}}{\sqrt{l_1^2 + l_2^2}} \end{bmatrix}^\top \quad (6)$$

where $\mathbf{l} = [l_1 \ l_2 \ l_3]^\top$ is the projected 2D image line from 3D line ${}^I\mathbf{x}_l$ in the IMU frame, $\mathbf{x}_s = [u_1, v_1, 1]^\top$ and $\mathbf{x}_e = [u_2, v_2, 1]^\top$ represent the homogeneous image coordinates.

D. Plane Measurements

Given point cloud from sensors (e.g., RGBD camera or LiDAR), we can directly extract planes. Therefore, we assume a direct plane measurement model as:

$$\mathbf{z}_\pi = {}^I\mathbf{x}_\pi + \mathbf{n}^{(\pi)} \quad (7)$$

where ${}^I\mathbf{x}_\pi$ is the plane in the IMU frame and $\mathbf{n}^{(\pi)}$ is the zero-mean white Gaussian noise.

E. Observability Analysis

Observability analysis for the linearized aided INS can be performed in a similar way as in [4], [11]. In particular, the observability matrix $\mathbf{M}(\mathbf{x})$ is given by:

$$\mathbf{M}(\mathbf{x}) = \begin{bmatrix} \mathbf{H}_{x,1}\Phi_{(1,1)} \\ \vdots \\ \mathbf{H}_{x,k}\Phi_{(k,1)} \end{bmatrix} \quad (8)$$

where $\mathbf{H}_{x,k}$ represents the measurement Jacobians at time-step k . The right null space of $\mathbf{M}(\mathbf{x})$, denoted by \mathbf{N} , indicates the unobservable directions of the underlying system.

III. UNIFIED FEATURE REPRESENTATIONS OF POINTS, LINES AND PLANES

As proper representations of point, line and plane features are important for state estimation, based on the extensive review of the most commonly used point, line and plane representations as summarized in Table I and Fig. 1, we introduce two sets of *unified* representations for points, lines and planes, i.e., the quaternion and CP parameterizations.

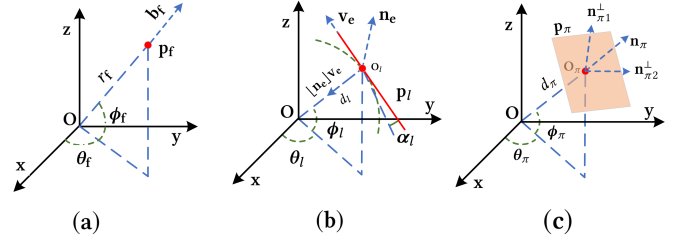


Fig. 1. Geometrical parameters for (a) point \mathbf{x}_f , (b) line \mathbf{x}_l , and (c) plane \mathbf{x}_π .

A. Point Representations

Model 1 in Table I is the homogeneous coordinates, f_i , $i \in 1 \dots 4$, for a point feature \mathbf{x}_f , which is the most general form. Model 2 represents the point with a unit bearing vector \mathbf{b}_f and a range scalar r_f measuring the distance from point to the origin \mathbf{O} (see Fig. 1 (a)). Since the 3D unit vector \mathbf{b}_f can be represented by 2 angles θ_f and ϕ_f : $\mathbf{b}_f = [\cos \theta_f \cos \phi_f \ \sin \theta_f \cos \phi_f \ \sin \phi_f]^\top$, we can easily derive Model 3, which is similar to spherical coordinate. If we use the inverse of range scalar $\lambda_f = \frac{1}{d_f}$, we get Model 4, which essentially is the inverse depth representation [33]. Recently, Maley and Huang [34] introduced a unit quaternion representation (Model 5) for points, which wraps \mathbf{b}_f and r_f into a unit quaternion. Model 5 leverages the quaternion error state, which is minimal for point state estimation. For example, a point in quaternion form can be written as:

$$\bar{q}_f = \begin{bmatrix} \mathbf{q}_f \\ q_f \end{bmatrix} = \frac{1}{\sqrt{1+r_f^2}} \begin{bmatrix} \mathbf{b}_f \\ r_f \end{bmatrix} \simeq \delta \bar{q}_f \otimes \hat{q}_f = \begin{bmatrix} \frac{1}{2} \delta \theta_f \\ 1 \end{bmatrix} \otimes \hat{q}_f \quad (9)$$

where $\delta \theta_f$ is the error state for point in unit quaternion form. Let \mathbf{p}_f be the closest point from the point to the origin, which is the most conventional parameterization for point feature (i.e., Model 6). It can be computed by multiplying the bearing vector \mathbf{b}_f with the range scalar r_f as:

$$\mathbf{p}_f = r_f \mathbf{b}_f = \hat{\mathbf{p}}_f + \tilde{\mathbf{p}}_f \quad (10)$$

where $\tilde{\mathbf{p}}_f$ is the error state in closest point form.

B. Line Representations

Given two points \mathbf{p}_{f1} and \mathbf{p}_{f2} in a line \mathbf{x}_l , we can obtain its Plücker coordinate (Model 1 of lines in Table I) as [28], [35]:

$$\begin{bmatrix} \mathbf{n}_l \\ \mathbf{v}_l \end{bmatrix} = \begin{bmatrix} [\mathbf{p}_{f1} \ \mathbf{p}_{f2}] \\ \mathbf{p}_{f2} - \mathbf{p}_{f1} \end{bmatrix} \quad (11)$$

where \mathbf{n}_l represents the normal direction of the plane constructed by the two points and the origin, \mathbf{v}_l represents the line direction. In Model 1, the distance from the origin to the line can be computed as $d_l = \frac{\|\mathbf{n}_l\|}{\|\mathbf{v}_l\|}$. Bartoli et al. [28] introduced the minimal orthonormal error state ($\delta \theta_l$ and $\delta \phi_l$, see [1] for detailed explanations) of Model 1 when involving lines in structure from motion. We can also represent the line with Model 2, which contains all the geometrical elements of a line, including a unit normal direction $\mathbf{n}_e = \frac{\mathbf{n}_l}{\|\mathbf{n}_l\|}$, a unit

TABLE I
SUMMARY OF POINT, LINE AND PLANE REPRESENTATIONS

Model #	Point	Error states	Line	Error states	Plane	Error states
1: General Form	f_1, f_2, f_3, f_4	not minimal	$\mathbf{n}_l, \mathbf{v}_l$	$\delta\theta_l, \delta\phi_l$	$\pi_1, \pi_2, \pi_3, \pi_4$	not minimal
2: Geometrical Form	\mathbf{b}_r, r_r	not minimal	$\mathbf{n}_e = \frac{\mathbf{n}_l}{\ \mathbf{n}_l\ }, \mathbf{v}_e = \frac{\mathbf{v}_l}{\ \mathbf{v}_l\ }, d_l = \frac{\ \mathbf{n}_l\ }{\ \mathbf{v}_l\ }$	not minimal	\mathbf{n}_π, d_π	not minimal
3: Spherical Form	θ_r, ϕ_r, r_r	$\tilde{\theta}_r, \tilde{\phi}_r, \tilde{r}_r$	$\theta_l, \phi_l, \alpha_l, d_l$	$\tilde{\theta}_l, \tilde{\phi}_l, \tilde{\alpha}_l, \tilde{d}_l$	$\theta_\pi, \phi_\pi, d_\pi$	$\tilde{\theta}_\pi, \tilde{\phi}_\pi, \tilde{d}_\pi$
4: Inverse Depth	$\theta_r, \phi_r, \lambda_r = \frac{1}{r_r}$	$\tilde{\theta}_r, \tilde{\phi}_r, \tilde{\lambda}_r$	$\theta_l, \phi_l, \alpha_l, \lambda_l = \frac{1}{d_l}$	$\tilde{\theta}_l, \tilde{\phi}_l, \tilde{\alpha}_l, \tilde{\lambda}_l$	$\theta_\pi, \phi_\pi, \lambda_\pi = \frac{1}{d_\pi}$	$\tilde{\theta}_\pi, \tilde{\phi}_\pi, \tilde{\lambda}_\pi$
5: Quaternion	$\tilde{q}_r = \frac{1}{\sqrt{1+r_r^2}} \begin{bmatrix} \mathbf{b}_r \\ r_r \end{bmatrix}$	$\delta\theta_r$	d_l, \tilde{q}_l with $\mathbf{R}(\tilde{q}_l) = [\mathbf{n}_e, \mathbf{v}_e, \mathbf{n}_e, \mathbf{v}_e]$	$\delta\theta_l, \tilde{d}_l$	$\tilde{q}_\pi = \frac{1}{\sqrt{1+d_\pi^2}} \begin{bmatrix} \mathbf{n}_\pi \\ d_\pi \end{bmatrix}$	$\delta\theta_\pi$
6: Closest Point	$\mathbf{p}_r = r_r \mathbf{b}_r$	$\mathbf{p}_r = \hat{\mathbf{p}}_r + \tilde{\mathbf{p}}_r$	$\mathbf{p}_l = d_l \tilde{q}_l$	$\mathbf{p}_l = \hat{\mathbf{p}}_l + \tilde{\mathbf{p}}_l$	$\mathbf{p}_\pi = d_\pi \mathbf{n}_\pi$	$\mathbf{p}_\pi = \hat{\mathbf{p}}_\pi + \tilde{\mathbf{p}}_\pi$

line direction $\mathbf{v}_e = \frac{\mathbf{v}_l}{\|\mathbf{v}_l\|}$ and the distance scalar d_l (see Fig. 1 (b)). Alternatively, a line can be parameterized by 3 angles $\theta_l, \phi_l, \alpha_l$ and a distance d_l (Model 3, see our companion technical report [36] for the transformation between Models 2 and 3). In analogy to the case of point features, we can use the inverse depth ($\lambda_l = \frac{1}{d_l}$) representation (Model 4) for line features. Interestingly, Kottas et al. [20] used a unit quaternion \tilde{q}_l and a distance scalar d_l to represent a line (Model 5), where the quaternion describes the line direction:

$$\mathbf{R}(\tilde{q}_l) = \begin{bmatrix} \mathbf{n}_e & \mathbf{v}_e & \mathbf{n}_e, \mathbf{v}_e \end{bmatrix} \quad (12)$$

$$\tilde{q}_l \simeq \delta\tilde{q}_l \otimes \hat{q}_l = \begin{bmatrix} \frac{1}{2}\delta\theta_l \\ 1 \end{bmatrix} \otimes \hat{q}_l \quad (13)$$

where $\delta\theta_l$ represents the error state of the line quaternion. The 4D minimal error states of the line include the quaternion error angle and the distance scalar error: $[\delta\theta_l^\top \ \tilde{d}_l]^\top$.

More importantly, if we multiply the unit quaternion \tilde{q}_l with the distance scalar d_l , we obtain a 4D vector, which can be considered as the ‘‘closest point’’ for a line in the 4D vector space (i.e., Model 6):

$$\mathbf{p}_l = d_l \tilde{q}_l = d_l \begin{bmatrix} \mathbf{q}_l^\top & q_l \end{bmatrix}^\top = \hat{\mathbf{p}}_l + \tilde{\mathbf{p}}_l \quad (14)$$

where $\tilde{\mathbf{p}}_l$ is the 4D error state for the closest point of a line. It should be noted that this minimal CP parameterization for lines (14) appears to be proposed for the first time and is shown to have good numerical stability (see Section VI).

C. Plane Representations

Similar to point features, the homogeneous coordinate ($f_i, i \in 1 \dots 4$) is the most general form for planes (Model 1) [37]. The Hesse form (Model 2) uses the normal direction \mathbf{n}_π and the distance scalar d_π to represent a plane. As \mathbf{n}_π can be represented by two angles θ_π and ϕ_π (see Fig. 1 (c)): $\mathbf{n}_\pi = \begin{bmatrix} \cos\theta_\pi \cos\phi_\pi & \sin\theta_\pi \cos\phi_\pi & \sin\phi_\pi \end{bmatrix}^\top$, the spherical coordinate (Model 3) can be used to represent the plane with two angles (θ_π and ϕ_π) and the distance scalar d_π . If using the inverse depth $\lambda_\pi = \frac{1}{d_\pi}$, we have the inverse depth representation for planes (Model 4). Recently, Kaess [29] proposed to use a unit quaternion to represent a plane by including the unit normal direction and the distance scalar

into a quaternion (Model 5):

$$\tilde{q}_\pi = \begin{bmatrix} \mathbf{q}_\pi \\ q_\pi \end{bmatrix} = \frac{1}{\sqrt{1+d_\pi^2}} \begin{bmatrix} \mathbf{n}_\pi \\ d_\pi \end{bmatrix} \simeq \delta\tilde{q}_\pi \otimes \hat{q}_\pi = \begin{bmatrix} \frac{1}{2}\delta\theta_\pi \\ 1 \end{bmatrix} \otimes \hat{q}_\pi \quad (15)$$

where $\delta\theta_\pi$ is the minimal error state for the quaternion plane representation. In Model 6, the closest point from the plane to the origin is used to represent the plane [27], [38] which has the minimal Euclidean error state $\tilde{\mathbf{p}}_\pi$:

$$\mathbf{p}_\pi = d_\pi \mathbf{n}_\pi = \hat{\mathbf{p}}_\pi + \tilde{\mathbf{p}}_\pi \quad (16)$$

D. Remarks

It is clear that Models 1 and 2 parameterizations for point, line and plane features, are not minimal, which may cause numerical issues (e.g., singular information matrices) if directly using these parameters during least-squares optimization. While Models 3 and 4 are minimal representations, these models might suffer from singularities when the elevation angle $\phi = \pm\frac{\pi}{2}$, similar to gimbal lock for Euler angles.

Interestingly, all point [34], line [20] and plane [29] features can be parameterized by the *unified* representation of quaternion (Model 5), which exploits the minimal error states of quaternion for state estimation for better numerical stability. However, the observability properties of quaternion representation for point and planes are missing in the literature, though those are studied in the case of line features in [20]. Therefore, we perform an extensive observability analysis with the unified quaternion representation for points, lines and planes, where we have analytically derive the measurement Jacobians (see our companion technical report [36] for detailed derivations), showing that the same observability properties of aided INS are preserved.

More importantly, the closest point (CP) form (i.e., Model 6) provides another *unified* parameterization for different geometrical features. The CP model for point is simply its 3D position in Euclidean space. While the CP representation for planes was introduced for INS in our prior work [27], in this work, we propose a novel 4D CP model for line features with the minimal 4D error states in 4D Euclidean space. Note that when using the CP parameterization, the error propagation for different geometrical features can be easily defined in the Euclidean vector space, and thus the cost functions of intuitive geometric interpretation can be formulated. In the following we will first perform detailed observability analysis using this novel CP line.

IV. OBSERVABILITY ANALYSIS FOR CP LINES

From the preceding section, it is not hard to find the connection between the error state $\tilde{\mathbf{p}}_l$ of a CP line and that of the corresponding quaternion line $[\delta\theta_l^T \quad \tilde{d}_l]^T$ [see (14)]:

$$\begin{aligned} \mathbf{p}_l &= \hat{\mathbf{p}}_l + \tilde{\mathbf{p}}_l = (\hat{d}_l + \tilde{d}_l) \delta\tilde{q}_l \otimes \hat{q} = (\hat{d}_l + \tilde{d}_l) \mathfrak{R}(\hat{q}) \begin{bmatrix} \frac{1}{2} \delta\theta_l \\ 1 \end{bmatrix} \\ \Rightarrow \mathfrak{R}(\hat{q})^T (\hat{\mathbf{p}}_l + \tilde{\mathbf{p}}_l) &= \begin{bmatrix} \frac{1}{2}(\hat{d}_l + \tilde{d}_l) \delta\theta_l \\ \hat{d}_l + \tilde{d}_l \end{bmatrix} \simeq \begin{bmatrix} \frac{1}{2} \hat{d}_l \delta\theta_l \\ \hat{d}_l + \tilde{d}_l \end{bmatrix} \\ \Rightarrow \mathfrak{R}(\hat{q})^T (\hat{\mathbf{p}}_l + \tilde{\mathbf{p}}_l) - \begin{bmatrix} \mathbf{0} \\ \hat{d}_l \end{bmatrix} &\simeq \begin{bmatrix} \frac{1}{2} \hat{d}_l \mathbf{I}_3 & 0 \\ 0 & 1 \end{bmatrix} \begin{bmatrix} \delta\theta_l \\ \tilde{d}_l \end{bmatrix} \\ \Rightarrow \begin{bmatrix} \delta\theta_l \\ \tilde{d}_l \end{bmatrix} &\simeq \begin{bmatrix} \frac{2}{\hat{d}_l} \mathbf{I}_3 & 0 \\ 0 & 1 \end{bmatrix} \left(\mathfrak{R}(\hat{q})^T (\hat{\mathbf{p}}_l + \tilde{\mathbf{p}}_l) - \begin{bmatrix} \mathbf{0} \\ \hat{d}_l \end{bmatrix} \right) \\ \Rightarrow \begin{bmatrix} \delta\theta_l \\ \tilde{d}_l \end{bmatrix} &\simeq \begin{bmatrix} \frac{2}{\hat{d}_l} (\hat{q}_l \mathbf{I}_3 - [\hat{\mathbf{q}}_l]) & -\frac{2}{\hat{d}_l} \hat{\mathbf{q}}_l \\ \hat{\mathbf{q}}_l^T & \hat{q}_l \end{bmatrix} \tilde{\mathbf{p}}_l \end{aligned} \quad (17)$$

where $\mathfrak{R}(\cdot)$ is the right quaternion multiplication matrix [32].

With the above relationship (17), we are now ready to perform observability properties of the aided INS with the CP-parameterized lines. In analogy to [1], [4], we consider the state vector with one CP line, which is given by:

$$\mathbf{x} = \begin{bmatrix} \mathbf{x}_l^T & \mathbf{p}_l^T \end{bmatrix}^T \quad (18)$$

The measurement Jacobians of the line measurement model (6) can be computed using the chain rule of differentiation:

$$\begin{aligned} \mathbf{H}_{\mathbf{x}}^{(l)} &= \frac{\partial \tilde{\mathbf{z}}_l}{\partial \tilde{\mathbf{x}}} = \begin{bmatrix} \frac{\partial \tilde{z}_l}{\partial \tilde{\mathbf{x}}_l} & \vdots & \frac{\partial \tilde{z}_l}{\partial \tilde{q}_l} \end{bmatrix} \\ &= \begin{bmatrix} \frac{\partial \tilde{z}_l}{\partial \tilde{\mathbf{I}}} \frac{\partial \tilde{\mathbf{I}}}{\partial \tilde{\mathbf{L}}} \frac{\partial \tilde{\mathbf{L}}}{\partial \tilde{\mathbf{x}}_l} & \vdots & \frac{\partial \tilde{z}_l}{\partial \tilde{\mathbf{I}}} \frac{\partial \tilde{\mathbf{I}}}{\partial \tilde{\mathbf{L}}} \frac{\partial \tilde{\mathbf{L}}}{\partial \tilde{q}_l} \frac{\partial \tilde{q}_l}{\partial \tilde{q}_l} \frac{\partial \begin{bmatrix} \delta\theta_l \\ \tilde{d}_l \end{bmatrix}}{\partial \tilde{q}_l} \end{bmatrix} \end{aligned} \quad (19)$$

where we have used the following identities (see [36]):

$$\mathbf{l} = \begin{bmatrix} \mathbf{K} & \mathbf{0}_3 \end{bmatrix}^T \mathbf{L} \quad (21)$$

$${}^l \mathbf{L} = \begin{bmatrix} {}^l \mathbf{n}_e & {}^l d_l \\ {}^l \mathbf{v}_e \end{bmatrix} = \begin{bmatrix} {}^l \mathbf{G} \mathbf{R} & -{}^l \mathbf{G} \mathbf{R} [{}^G \mathbf{p}_l] \\ \mathbf{0}_3 & {}^l \mathbf{G} \mathbf{R} \end{bmatrix} \begin{bmatrix} {}^G \mathbf{n}_e & {}^G d_l \\ {}^G \mathbf{v}_e \end{bmatrix} \quad (22)$$

$$\frac{\partial \tilde{z}_l}{\partial \tilde{\mathbf{I}}} = \frac{1}{l_n} \begin{bmatrix} u_1 - \frac{l_1 e_1}{l_n^2} & v_1 - \frac{l_2 e_1}{l_n^2} & 1 \\ u_2 - \frac{l_1 e_2}{l_n^2} & v_2 - \frac{l_2 e_2}{l_n^2} & 1 \end{bmatrix} \quad (23)$$

where $e_1 = \mathbf{I}^T \mathbf{x}_s$, $e_2 = \mathbf{I}^T \mathbf{x}_e$ and \mathbf{K} is the projection matrix for lines. The detailed derivations can be found in [36]. In particular, if using lines, $\Phi_{\text{feat}} = \mathbf{I}_4$, then we can have the k -th block of observability matrix as:

$$\begin{aligned} \mathbf{M}_k^{(l)} &= \mathbf{H}_{\mathbf{x}k}^{(l)} \Phi(k, 1) = \frac{\partial \tilde{z}_l}{\partial \tilde{\mathbf{I}}} \begin{bmatrix} \mathbf{K}^T \mathbf{G} \mathbf{R} & \mathbf{0}_3 \end{bmatrix} \times \\ &\begin{bmatrix} \Gamma_{111} & \Gamma_{112} & \Gamma_{113} & \Gamma_{114} & \Gamma_{115} & \Gamma_{116} & \Gamma_{117} \\ \Gamma_{121} & \Gamma_{122} & \Gamma_{123} & \Gamma_{124} & \Gamma_{125} & \Gamma_{126} & \Gamma_{127} \end{bmatrix} \end{aligned} \quad (24)$$

where $\Gamma_{lij}, i \in 1 \dots 2, j = 1 \dots 7$ can again be found in our companion technical report [36]. Based on this structure of the observability matrix, we conclude as follows:

Lemma 1. *For aided INS, if there is only one line feature in the state vector, and the line feature is parameterized in the proposed 4D CP form, the system will have at least 5 unobservable directions denoted by $\mathbf{N}^{(l)}$:*

$$\mathbf{N}^{(l)} = \begin{bmatrix} {}^l \mathbf{R}^G \mathbf{g} & \mathbf{0}_3 & \mathbf{0}_{3 \times 1} \\ \mathbf{0}_{3 \times 1} & \mathbf{0}_3 & {}^G \hat{\mathbf{v}}_e \\ -[{}^G \hat{\mathbf{v}}_l]^G \mathbf{g} & \mathbf{0}_3 & \mathbf{0}_{3 \times 1} \\ \mathbf{0}_{3 \times 1} & \mathbf{0}_3 & \mathbf{0}_{3 \times 1} \\ -[{}^G \hat{\mathbf{p}}_l]^G \mathbf{g} & {}^L \mathbf{R} & \mathbf{0}_{3 \times 1} \\ -\frac{{}^G \hat{d}_\pi}{2} ({}^G \hat{q}_l \mathbf{I}_3 - [{}^G \hat{\mathbf{q}}_l])^G \mathbf{g} & \mathbf{N}_{la} & \mathbf{0}_{3 \times 1} \\ \frac{{}^G \hat{d}_l}{2} {}^G \hat{\mathbf{q}}_l^T \mathbf{G} \mathbf{g} & \mathbf{N}_{lb} & 0 \end{bmatrix} \quad (25)$$

where we have employed:

$${}^L \mathbf{R} = \begin{bmatrix} {}^G \hat{\mathbf{n}}_e & {}^G \hat{\mathbf{v}}_e & [{}^G \hat{\mathbf{n}}_e]^G \hat{\mathbf{v}}_e \end{bmatrix} \quad (26)$$

$$\mathbf{N}_{la} = \begin{bmatrix} \frac{1}{2} ({}^G \hat{q}_l \mathbf{I}_3 - [{}^G \hat{\mathbf{q}}_l])^G \hat{\mathbf{v}}_e & \mathbf{0}_{3 \times 1} & -{}^G \hat{\mathbf{q}}_l \end{bmatrix} \quad (27)$$

$$\mathbf{N}_{lb} = \begin{bmatrix} -\frac{1}{2} {}^G \hat{\mathbf{q}}_l^T {}^G \hat{\mathbf{v}}_e & 0 & -{}^G \hat{q}_l \end{bmatrix} \quad (28)$$

Proof. See [?]. \square

Let $\mathbf{N}_i^{(l)}, i \in 1 \dots 5$ denote the i -th column of the matrix $\mathbf{N}^{(l)}$. $\mathbf{N}_1^{(l)}$ relates to the global yaw around the gravity direction, $\mathbf{N}_{2:4}^{(l)}$ associate with the global position of the sensor platform, and $\mathbf{N}_5^{(l)}$ corresponds to the velocity along the line direction. Clearly, the proposed CP line representation preserves the system observability properties [1].

V. OBSERVABILITY ANALYSIS FOR AIDED INS WITH HETEROGENEOUS FEATURES

In this section, we study the observability properties for the general aided INS with the combination of different geometrical features including points, lines and planes that are all in the unified representation of CP form. To keep concise presentation, we here consider one feature of each type in the state vector, i.e., $\mathbf{x}_{\text{feat}} = \begin{bmatrix} {}^G \mathbf{p}_f^T & {}^G \mathbf{p}_l^T & {}^G \mathbf{p}_\pi^T \end{bmatrix}^T$. The state vector of the system then becomes:

$$\mathbf{x} = \begin{bmatrix} \mathbf{x}_l^T & {}^G \mathbf{p}_f^T & {}^G \mathbf{p}_l^T & {}^G \mathbf{p}_\pi^T \end{bmatrix}^T \quad (29)$$

The measurement model stacks (5), (6) and (7):

$$\mathbf{z}_{pl\pi} = \begin{bmatrix} \mathbf{z}_p^T & \mathbf{z}_l^T & \mathbf{z}_\pi^T \end{bmatrix}^T \quad (30)$$

The state transition matrix for the feature state becomes $\Phi_{\text{feat}} = \mathbf{I}_{10}$. Proceeding similarly, we can construct the observability matrix and then compute its null space in order to find the unobservable directions:

Lemma 2. *For the aided INS with one point, one line and one plane feature in the state vector and they are all*

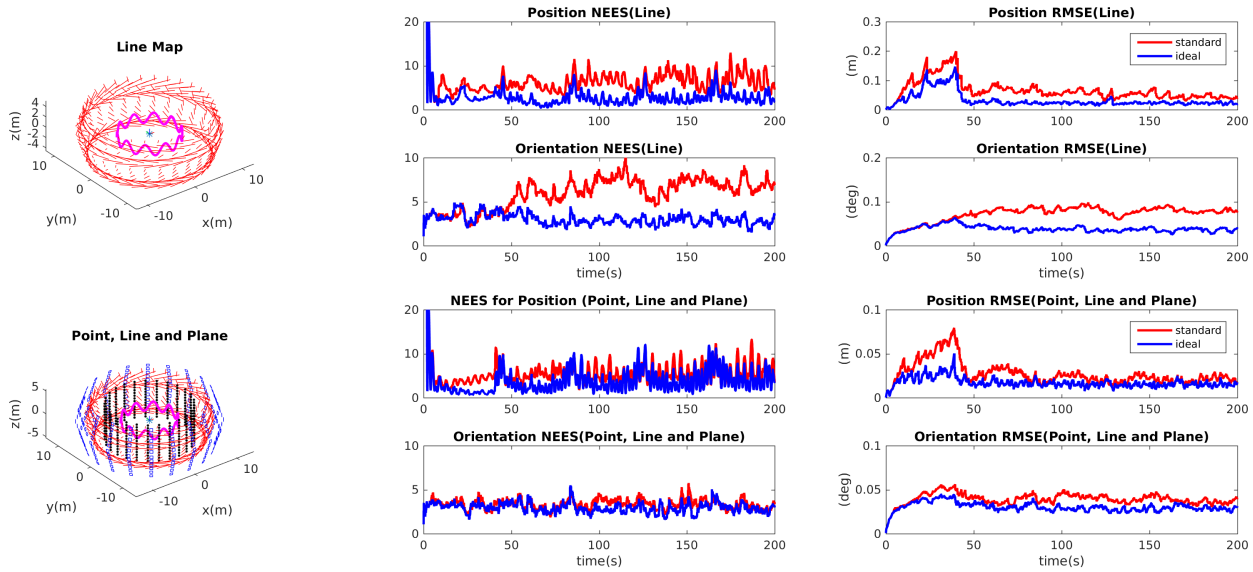


Fig. 2. Monte Carlo results of the standard and ideal EKFs for vision-aided inertial SLAM (VI-SLAM): (left) simulation setup, (middle) NEES of sensor pose (position and orientation), and (right) RMSE of sensor pose (position and orientation).

parameterized in CP form, the system will have at least 4 unobservable directions as $\mathbf{N}^{(pl\pi)}$.

$$\mathbf{N}^{(pl\pi)} = \begin{bmatrix} I_1 \hat{\mathbf{R}}^G \mathbf{g} & \mathbf{0}_3 \\ \mathbf{0}_{3 \times 1} & \mathbf{0}_3 \\ -[{}^G \hat{\mathbf{v}}_l \times] {}^G \mathbf{g} & \mathbf{0}_3 \\ \mathbf{0}_{3 \times 1} & \mathbf{0}_3 \\ -[{}^G \hat{\mathbf{p}}_k \times] {}^G \mathbf{g} & {}^G_L \hat{\mathbf{R}} \\ -[{}^G \hat{\mathbf{p}}_r \times] {}^G \mathbf{g} & {}^G_L \hat{\mathbf{R}} \\ -\frac{{}^G \hat{d}_l}{2} ({}^G \hat{\mathbf{q}}_l \mathbf{I}_3 - [{}^G \hat{\mathbf{q}}_l]) {}^G \mathbf{g} & \mathbf{N}_{la} \\ \frac{{}^G \hat{d}_l}{2} {}^G \hat{\mathbf{q}}_l {}^G \mathbf{g} & \mathbf{N}_{lb} \\ -[{}^G \hat{\mathbf{p}}_\pi] {}^G \mathbf{g} & {}^G \hat{\mathbf{n}}_\pi \mathbf{e}_3 {}^T {}^G \hat{\mathbf{R}} {}^T {}^G \hat{\mathbf{R}} \end{bmatrix} \quad (31)$$

where we have defined ${}^G \mathbf{R} = [{}^G \mathbf{n}_{\pi 1} \quad {}^G \mathbf{n}_{\pi 2} \quad {}^G \mathbf{n}_\pi]$, and ${}^G \mathbf{n}_{\pi i}$, $i = 1, 2$ are orthonormal to ${}^G \mathbf{n}_\pi$ (see Fig. 1).

Proof. See [36]. \square

VI. SIMULATION RESULTS

We have performed extensively Monte Carlo simulations of EKF-based visual-inertial SLAM to validate the proposed CP parameterization for line as well as the observability analysis for aided INS with the combination of geometrical features all in unified CP form. An IMU with a stereo camera moving along a 3D sinusoid trajectory is simulated. The stereo camera produces the projective feature measurements from a pre-generated map. To validate the observability analysis, we have two different EKFs as in [4], [11], [39]: (i) the ideal EKF-based VINS which uses true states as linearization points, and (ii) the standard EKF-based VINS which uses estimated states for linearization. The ideal EKF should demonstrate consistent estimation, while the standard EKF tends to be overconfident and thus, inconsistent. The normalized estimation error squared (NEES) and root mean squared error (RMSE) are used to evaluate the consistency and accuracy [40] of the estimator. It is clear from Fig. 2

that the standard VINS with line features in proposed 4D CP form can generate accurate estimation results. In addition, as expected, the ideal EKF, which is consistent, performs better than the standard EKF, for the VINS with the combination of geometrical features in CP form. Note that by marginalizing features through null space operation [41], we have also extended the standard MSCKF VIO with point features [2] to the case of heterogeneous features and validated its performance in simulations as shown in [36].

VII. CONCLUSIONS AND FUTURE WORK

In this paper, we have introduced two sets of unified representations for different geometrical features (points, lines and planes): the quaternion form and the CP form. We particularly advocate a novel CP model to parameterize line features, of which the error states are directly in the minimal 4D Euclidean vector space. Moreover, based on our recent work [1], we have provided an extensive observability analysis together with all the analytically computed Jacobians for aided INS with geometrical features in unified representations, showing that both representations preserve the same observability properties. In particular, the proposed unified CP representation and the observability analysis are validated through extensive Monte-Carlo simulations of vision-aided INS. In the future, we will investigate the (stochastic) observability of aided INS under adversarial attacks [42] or unknown inputs [43] in order to design secure estimators for robot navigation. In addition, based on the quaternion parameterization, we can extend this representation in $SO(3)$ form, and build visual-inertial SLAM system to compare these representations for different geometrical features.

REFERENCES

- [1] Y. Yang and G. Huang, "Aided inertial navigation with geometric features: Observability analysis," in *Proc. of the IEEE International Conference on Robotics and Automation*, Brisbane, Australia, May 21–25, 2018, pp. 2334–2340.

- [2] A. I. Mourikis and S. I. Roumeliotis, "A multi-state constraint Kalman filter for vision-aided inertial navigation," in *International Conference on Robotics and Automation*, Rome, Italy, Apr. 10–14, 2007, pp. 3565–3572.
- [3] Y. Yang and G. Huang, "Acoustic-inertial underwater navigation," in *Proc. of the IEEE International Conference on Robotics and Automation*, Singapore, May 29–Jun.3, 2017, pp. 4927–4933.
- [4] J. Hesch, D. Kottas, S. Bowman, and S. Roumeliotis, "Consistency analysis and improvement of vision-aided inertial navigation," *IEEE Transactions on Robotics*, vol. PP, no. 99, pp. 1–19, 2013.
- [5] M. Li and A. I. Mourikis, "High-precision, consistent EKF-based visual-inertial odometry," *International Journal of Robotics Research*, vol. 32, no. 6, pp. 690–711, 2013.
- [6] S. Leutenegger, S. Lynen, M. Bosse, R. Siegwart, and P. Furgale, "Keyframe-based visual-inertial odometry using nonlinear optimization," *International Journal of Robotics Research*, Dec. 2014.
- [7] G. Huang, M. Kaess, and J. Leonard, "Towards consistent visual-inertial navigation," in *IEEE International Conference on Robotics and Automation*, Hong Kong, China, May 31–Jun. 7 2014, pp. 4926–4933.
- [8] T. Qin, P. Li, and S. Shen, "Vins-mono: A robust and versatile monocular visual-inertial state estimator," *arXiv preprint arXiv:1708.03852*, 2017.
- [9] K. Eickenhoff, P. Geneva, and G. Huang, "Direct visual-inertial navigation with analytical preintegration," in *Proc. of the IEEE International Conference on Robotics and Automation*, Singapore, May 29–Jun.3, 2017, pp. 1429–1435.
- [10] Z. Huai and G. Huang, "Robocentric visual-inertial odometry," in *Proc. IEEE/RSJ International Conference on Intelligent Robots and Systems*, Madrid, Spain, Oct. 1–5 2018.
- [11] G. Huang, A. I. Mourikis, and S. I. Roumeliotis, "Observability-based rules for designing consistent EKF SLAM estimators," *International Journal of Robotics Research*, vol. 29, no. 5, pp. 502–528, Apr. 2010.
- [12] T. Zhang, K. Wu, J. Song, S. Huang, and G. Dissanayake, "Convergence and consistency analysis for a 3-d invariant-ekf slam," *IEEE Robotics and Automation Letters*, vol. 2, no. 2, pp. 733–740, April 2017.
- [13] Y. Bar-Shalom, X. R. Li, and T. Kirubarajan, *Estimation with Applications to Tracking and Navigation*. New York: John Wiley and Sons, 2001.
- [14] G. Huang, "Improving the consistency of nonlinear estimators: Analysis, algorithms, and applications," Ph.D. dissertation, Department of Computer Science and Engineering, University of Minnesota, 2012. [Online]. Available: <http://people.csail.mit.edu/ghuang/paper/thesis.pdf>
- [15] A. Martinelli, "Visual-inertial structure from motion: Observability and resolvability," in *Proc. of the IEEE/RSJ International Conference on Intelligent Robots and Systems*, Tokyo, Japan, Nov. 2013, pp. 4235–4242.
- [16] K. J. Wu, C. X. Guo, G. Georgiou, and S. I. Roumeliotis, "Vins on wheels," in *International Conference on Robotics and Automation*. Singapore: IEEE, May. 2017, pp. 5155–5162.
- [17] A. Martinelli, "Vision and IMU data fusion: Closed-form solutions for attitude, speed, absolute scale, and bias determination," *IEEE Transactions on Robotics*, vol. 28, no. 1, pp. 44–60, 2012.
- [18] D. G. Kottas, J. A. Hesch, S. L. Bowman, and S. I. Roumeliotis, "On the consistency of vision-aided inertial navigation," in *International Symposium on Experimental Robotics*, Quebec City, Canada, Jun. 17–20, 2012.
- [19] H. Yu and A. I. Mourikis, "Vision-aided inertial navigation with line features and a rolling-shutter camera," in *International Conference on Robotics and Intelligent Systems*, Hamburg, Germany, October 2015, pp. 892–899.
- [20] D. G. Kottas and S. I. Roumeliotis, "Efficient and consistent vision-aided inertial navigation using line observations," in *International Conference on Robotics and Automation*, Karlsruhe, Germany, May 6–10 2013, pp. 1540–1547.
- [21] Y. He, J. Zhao, Y. Guo, W. He, , and K. Yuan, "PI vio: Tightly coupled monocular visual inertial odometry using point and line features," *Sensors*, 2018.
- [22] S. Heo, J. H. Jung, and C. G. Park, "Consistent ekf-based visual-inertial navigation using points and lines," *IEEE Sensors Journal*, 2018.
- [23] F. Zheng, G. Tsai, Z. Zhang, S. Liu, C.-C. Chu, and H. Hu, "PI-VIO: Robust and Efficient Stereo Visual Inertial Odometry using Points and Lines," *ArXiv e-prints*, Mar. 2018.
- [24] J. A. Hesch, F. M. Mirzaei, G. L. Mariottini, and S. I. Roumeliotis, "A laser-aided inertial navigation system (l-ins) for human localization in unknown indoor environments," in *International Conference on Robotics and Automation*, Anchorage, Alaska, May. 3 - 8 2010, pp. 5376–5382.
- [25] C. X. Guo and S. I. Roumeliotis, "Imu-rgbd camera navigation using point and plane features," in *International Conference on Intelligent Robots and Systems*, Tokyo, Japan, Nov. 3–7, 2013, pp. 3164–3171.
- [26] M. Hsiao, E. Westman, and M. Kaess, "Dense planar-inertial slam with structural constraints," in *Proc. of the IEEE International Conference on Robotics and Automation*, Brisbane, Australia, May. 21–25 2018, pp. 6521–6528.
- [27] P. Geneva, K. Eickenhoff, Y. Yang, and G. Huang, "LIPS: Lidar-inertial 3d plane slam," in *Proc. IEEE/RSJ International Conference on Intelligent Robots and Systems*, Madrid, Spain, Oct. 1–5 2018.
- [28] A. Bartoli and P. Sturm, "Structure from motion using lines: Representation, triangulation and bundle adjustment," *Computer Vision and Image Understanding*, vol. 100, no. 3, pp. 416–441, dec 2005.
- [29] M. Kaess, "Simultaneous localization and mapping with infinite planes," in *2015 IEEE International Conference on Robotics and Automation (ICRA)*, Seattle, Washington, May 2015, pp. 4605–4611.
- [30] Y. Yang and G. Huang, "Observability analysis for aided ins with heterogeneous features of points, lines and planes," RPNG, University of Delaware, Tech. Rep., 2018, udel.edu/~yuyang/downloads/tr.observabilityIII.pdf.
- [31] F. Nardi, B. Della Corte, and G. Grisetti, "Unified representation of heterogeneous sets of geometric primitives," in *Workshop of International Conference of Robotics and Automation*, Brisbane, AUS, 21–25 May 2018.
- [32] N. Trawny and S. I. Roumeliotis, "Indirect Kalman filter for 3D attitude estimation," University of Minnesota, Dept. of Comp. Sci. & Eng., Tech. Rep., Mar. 2005.
- [33] J. Civera, A. Davison, and J. Montiel, "Inverse depth parametrization for monocular SLAM," *IEEE Transactions on Robotics*, vol. 24, no. 5, pp. 932–945, Oct. 2008.
- [34] J. Maley and G. Huang, "Unit quaternion-based parameterization for point features in visual navigation," in *Proc. IEEE/RSJ International Conference on Intelligent Robots and Systems*, Madrid, Spain, Oct. 2018.
- [35] X. Zuo, J. Xie, Y. Liu, and G. Huang, "Robust visual SLAM with point and line features," in *Proc. of the IEEE/RSJ International Conference on Intelligent Robots and Systems*, Vancouver, Canada, Sep. 24–28, 2017.
- [36] Y. Yang and G. Huang, "Aided inertial navigation: Unified feature representations and observability analysis," RPNG, University of Delaware, Tech. Rep., 2019, udel.edu/~yuyang/downloads/tr.observabilityII.pdf.
- [37] R. Hartley and A. Zisserman, *Multiple View Geometry in Computer Vision*. Cambridge, U. K.: Cambridge University Press, 2000.
- [38] P. F. Proença and Y. Gao, "Probabilistic RGB-D odometry based on points, lines and planes under depth uncertainty," *CoRR*, vol. abs/1706.04034, 2017.
- [39] J. Hesch, D. Kottas, S. Bowman, and S. Roumeliotis, "Camera-IMU-based localization: Observability analysis and consistency improvement," *International Journal of Robotics Research*, vol. 33, pp. 182–201, 2014.
- [40] Y. Bar-Shalom and T. E. Fortmann, *Tracking and Data Association*. New York: Academic Press, 1988.
- [41] Y. Yang, J. Maley, and G. Huang, "Null-space-based marginalization: Analysis and algorithm," in *Proc. IEEE/RSJ International Conference on Intelligent Robots and Systems*, Vancouver, Canada, Sep. 24–28, 2017.
- [42] Y. Yang and G. Huang, "Map-based localization under adversarial attacks," in *Proc. of the International Symposium on Robotics Research*, Puerto Varas, Chile, Dec.11–14, 2017.
- [43] A. Martinelli, "Nonlinear unknown input observability: Extension of the observability rank condition," *IEEE Transactions on Automatic Control*, pp. 1–1, 2018.